Pattern Recognition 42 (2009) 141 – 146

Contents lists available at ScienceDirect

Pattern Recognition

journal homepage: www.elsevier.com/locate/pr

Automated cell analysis in 2D and 3D: A comparative study

Michael G. Meyer[a,*], Mark Fauver[b], J. Richard Rahn[a], Thomas Neumann[a], Florence W. Patten[a], Eric J. Seibel[c], Alan C. Nelson[a]

[a] VisionGate, Inc., 1509 56th Ave. Ct. NW, Gig Harbor, WA 98335, USA
[b] Nortis, Inc. 1509 56th Ave. Ct. NW, Gig Harbor, WA 98335, USA
[c] Department of Mechanical Engineering, University of Washington, 204 Fluke Hall, Box 352600, Seattle, WA 98195, USA

ARTICLE INFO

Article history:
Received 31 July 2007
Received in revised form 24 March 2008
Accepted 18 June 2008

Keywords:
Automated classification
3D
Cancer diagnosis
Tomography

ABSTRACT

Optical projection tomographic microscopy is a technique that allows 3D analysis of individual cells. Theoretically, 3D morphometry would more accurately capture cellular features than 2D morphometry. To evaluate this thesis, classifiers based on 3D reconstructions of cell nuclei were compared with 2D images from the same nuclei. Human adenocarcinoma and normal lung epithelium cells were used. Testing demonstrated a three-fold reduction in the false negative rate for adenocarcinoma detection in 3D versus 2D at the same high specificity. We conclude that 3D imaging will potentially expand the horizon for automated cell analysis with broad applications in the biological sciences.

1. Introduction and study hypothesis

In 2D representation of 3D objects, spheres become circles, pyramids become trapezoids, and lines remain lines, but of misleading length. Single perspective 2D imaging renders 3D objects incompletely, thus limiting the performance of automated classification systems that rely on 2D feature measurements. The technique of tomographic reconstruction [1] potentially removes this constraint and permits creation of a 3D model that can comprehensively represent the actual 3D features of an object based on its multiple 2D projections. Our hypothesis is that true 3D feature measurements of a 3D object will out-perform 2D feature measurements from a 2D image of a 3D object.

More specifically, our interest is in cellular classification to aid in early detection of lung cancer. We report here on a new form of microscopy that enables automated cell classification based on optical projection-based 3D computed tomography [2] (Cell-CT™), and establish its merit relative to classification performance based on 2D images using cancer and normal human lung cells in culture. Some considerations follow:

- A 3D image provides the dimension of depth: volume and surface areas may be computed accurately.
- A digital 3D tomographic reconstruction enables the creation of an additional host of descriptive 3D features that are not available in 2D.
- Features based on a single 2D perspective are orientation dependent and focal plane dependent.
- Conventional 2D optical microscopy that supports sub-micron resolution is not consistent with a depth of field that encompasses the thickness of a cell nucleus. Therefore, 2D imaging provides only a sample of the nuclear volume, omitting some potentially important nuclear characteristics [3].
- Objects in conventional 2D microscopy are sometimes occluded by overlapping material from higher and lower focal planes.
- Suspended cells imaged in 3D are more likely to conform to their *in situ* condition, whereas forcing a cell to lie flat against a glass slide, as in conventional 2D microscopy, likely introduces morphological distortions.

Our aim, therefore, is to conduct a test of the hypothesis that classification of a cell is more accurate when based on a 3D representation than a 2D sample. Construction of our test was organized to provide a 3D to 2D performance comparison free from specimen composition, specimen preparation and instrumentation bias. Consequently, we examined the relative performance difference between 2D and 3D classification results on the same cell objects. As such, comparisons of performance measures derived from multiple observers were avoided since experimental conditions may vary considerably from observer to observer.

The 3D imaging of cells may be achieved through several methods including: transmission electron microscopy [4] and confocal microscopy [5]. These methods produce high quality 3D

* Corresponding author. Tel.: +1 206 616 1465; fax: +1 206 685 4315.
E-mail addresses: meyer@visiongate3d.com (M.G. Meyer), m_fauver@yahoo.com (M. Fauver), rahn@visiongate3d.com (J.R. Rahn), neumann@visiongate3d.com (T. Neumann), patten@visiongate3d.com (F.W. Patten), eseibel@u.washington.edu (E.J. Seibel), nelson@visiongate3d.com (A.C. Nelson).

0031-3203/$ - see front matter © 2008 Elsevier Ltd. All rights reserved.
doi:10.1016/j.patcog.2008.06.018

renderings of cells but with non-isotropic resolution and at considerable expense in time and hardware cost. Therefore, we used the optical Cell-CT system for imaging cells, whose pipeline architecture for delivery of cells promotes rapid imaging necessary to create the cellular ensembles needed to test the classification hypothesis.

The sections below describe the methods for cell preparation and Cell-CT imaging, classification methods, experimental design, results and discussion.

2. Methods

2.1. Cell-CT system

To assess the differences between 3D and 2D imaging, we developed the optical Cell-CT system, which comprises:

- Cell fixation and absorption-based staining.
- Preparation to suspend cells in an optical-gel that is injected into a capillary tube.
- An optical platform capable of rendering projection images of cellular objects from multiple perspectives as the capillary tube rotates.
- Tomographic reconstruction using a filtered back-projection method similar to X-ray computed tomography.
- Automated feature extraction and classification to foster high-sensitivity and high-specificity characterization of cells.
- Visualization using standard volume rendering techniques.

Human lung adenocarcinoma (cell line A549) and normal human small airway epithelial cells (cell line SAEC) were grown in culture for the purpose of testing the Cell-CT system. Cells were fixed and stained using standard techniques involving 2% paraformaldehyde and Gill hematoxyln. Use of standard fixation and staining techniques permits cellular analysis that is consistent with the current standards of cell cytology, thus permitting an expert cytologist to perform standard cell morphological characterization when building databases used to train classifiers. Cells were enucleated to focus attention on cell nuclear features, although enucleation is not a requirement of operation of the Cell-CT.

A brief overview of the Cell-CT microscope is provided below and illustrated in Fig. 1. Stained nuclei were suspended in an optical-gel and injected into a capillary tube (50 μm inner diameter) that is optically coupled to an objective lens. Pressure applied to the gel moves objects into position for image collection as the tube rotates. As the objective lens plane of focus is swept through the object, focus-invariant images, or pseudo-projections, are taken that equally sample the entire nuclear volume from a single perspective. The pseudo-projection image is created rapidly compared to the tube rotation speed, such that motion-blur is negligible. A large set of pseudo-projections is taken from multiple views (by rotating the tube containing the cell) and then processed using a filtered back-projection algorithm to compute the tomographic reconstruction.

Fig. 1 illustrates pseudo-projections taken at three angular positions: 0°, 90° and 180°. Illumination was provided by inchoherent light in the visible portion of the spectrum. In the reconstruction, 3D voxels were cubic, with a size of 66.5 nm in each dimension. Reconstruction volumes varied in size, as the image collection volume was cropped around the object. Typically, volumes were approximately 150 pixels on the side. A total of 500 pseudo-projections were acquired at 0.72° increments around 360° of rotation. Optical settings were: source wavelength = 585 ± 30 nm, condenser NA = 0.4, objective NA = 1.3 and magnification = 100×. A 12-bit monochrome camera was used.

For each nucleus, a reference 2D image was also collected on the Cell-CT system using a single, fixed-position focal plane that was automatically and centrally focused.

2.2. Classification techniques

Automated cell classification involves numerically representing morphology markers that distinguish normal from abnormal cells. These markers were used as input features to a classifier that provides a statistical risk score that correlates to the probability of abnormality. Features were defined to represent morphological characteristics that, from 2D cytology, are known to distinguish normal from adenocarcinoma cell nuclei [6]. These features describe various aspects of nuclear morphology including size and shape, grey scale distribution, texture, nucleoli count and normalized features. A total of 65 features were computed for both 2D and 3D images in

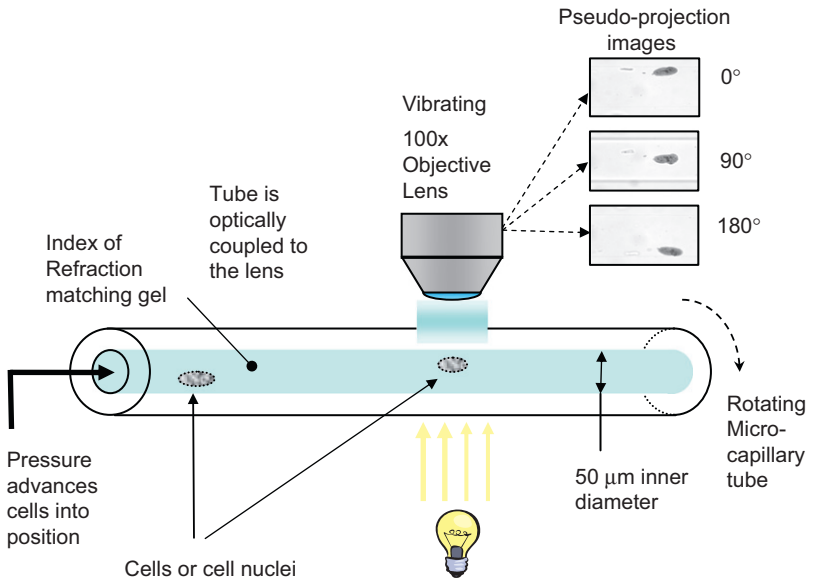

Fig. 1. Diagram illustrating operation of the optical projection Cell-CT system.

Table 1
Description of features used for classifier development

Type of feature	Number of features
Size and shape features—describing the shape of the object	7
Histogram features—describing the grey scale distribution associated with the 2D or 3D object	15
Texture features1—describing the general character of grey scale texture within the volume or area of the 2D or 3D object	20
Texture features2—characterizes texture based on the 2D or 3D fourier transform of the object	10
Nucleolar features—nucleoli are important features appearing more commonly in malignant nuclei. These features aim to characterize the occurrence of these structures	8
Normalized features—combinations of the above features, e.g. surface area/volume ratio	5
Total features	65

the study. By using features that have recognized significance for 2D cytology, we tested the hypothesis that the analogous 3D features might provide more accurate classification than the 2D features.

The set of 65 features used for the study is defined in Table 1.

It is important to note that the set of features employed for this study is not exhaustive of the possibilities either for 2D or 3D classification. There are many features that only have a 3D definition, for example, the count of surface permeations, or invaginations that lead into voids in the interior of the nucleus. An example of such a structure is given later in Section 3. The 2D slice would only capture these structures by happenstance, and even then a comprehensive measurement of these structures would not be possible. As 3D cellular morphology, and its relevance to the detection of pre-cancerous and cancerous conditions of the lung, is an evolving science, additional feature possibilities are sure to develop in the future. For the purposes of this comparative study, however, we restricted our 3D feature set so that each feature in the 2D set has a comparable definition in the 3D set. Also, there is additional complexity regarding the computation of features in 2D relative to 3D. The 2D features are based on the portion of the object in the image plane. In some cases, features in 3D, such as in the histogram features in Table 1, are based on the whole 3D object. For ease of computation, shape features in 3D were computed as the summation of values for all the slices that comprise the 3D object. For example, the surface area was computed, using erosions and subtractions, by finding the perimeter for the object in each slice and summing over all slices in the 3D volume. This technique can result in noise at the poles of the 3D object. It remains to be seen if 3D morphological processing would yield improvements in feature measurements that justify the additional computational complexity.

The classifier development followed the plan outlined below:

1. Image input—digital 2D images and 3D tomographic reconstructions of the cell nuclei to be classified were produced from the same cell.
2. Segmentation—the object of interest is extracted from the background.
3. Feature extraction—measurement of features of the object as defined by the segmentation mask. K features are defined to be a best guess to discriminate the classes.
4. Database—populate a database containing N normal and M abnormal objects. K features are computed for each object.
5. Feature selection—identify those J ($J<K$) features that best discriminate between normal and abnormal classes.
6. Classifier—combine J features into a single numeric risk score that expresses the likelihood that the object is abnormal.

Accurate segmentation is important since features are based on the pixels in the 2D image or 3D volume that correspond to the segmentation mask. Since hematoxyln stain is taken up by the nuclear envelope, typically there is a sharp gradient that separates the background grey level from that of the rim of the nucleus. Also, cells are presented one at a time; so therefore, it is not necessary to disentangle adjacent cells. Consequently, segmentation was a simple procedure, accomplished by threshold. This threshold was established by examining the histogram for the 2D image or 3D volume in question. Most of the pixels in the image or volume are associated with the background, and so this grey level may be discovered easily by finding the primary mode, or peak, of the grey scale histogram for the 2D or 3D image. Trial and error then yielded a small offset so that the final threshold value was 105% of the primary mode grey scale value. Segmentation was further refined by performing a connected components [7] algorithm on the resulting mask to remove spurious debris that might remain above the threshold for the primary object.

We selected the classification technique [8] to reduce over-specialization to training data. Over-specialization occurs when the classifier fits around sampled feature values in ways that do not reflect the true characteristics of the feature distributions. Our training results were checked for over-specialization using the leave-out-one method of cross-validation [9]. From the available features, non-parametric feature selection was performed to choose the features to be used in the classifier. Non-parametric feature selection [10] assures that no prior assumptions were made regarding the statistical distribution that characterized the features. Feature selection was done in an independent way for classifiers using one, two and three features and in a stepwise fashion [11] thereafter. Confidence intervals for sensitivity were established using the bootstrap method [12].

3. Experimental design

We tested the hypothetical advantage of 3D over 2D features by independently developing classifiers based on 3D tomographic reconstructions and fixed focal plane 2D images. The study was designed to eliminate cell population and preparation bias that could be introduced by performing the study on two different groups of cells. Therefore, a common group of cells was used for the collection of both a 2D image focused in the center of the nucleus and a set of pseudo-projection images to compute a 3D tomographic reconstruction. Moreover, a single set of features was defined in both 2D and 3D and a single method for the development of the classifier was used for both sets of data. Defining the study in this way allowed for isolation of performance differences to a single causal factor: the relative merits of 2D and 3D features. The study comprised 178 nuclei from adenocarcinoma cells and 148 nuclei from normal cells.

Tomographic reconstructions were further processed to render their features more apparent for visual inspection. Applying a threshold for opacity to render a noise free background produced the object surface. Opacity for the object interior was graded based on the grey scale histogram. Chromatic contrast was applied to further enhance appreciation of sub-nuclear features, such as a nucleolus. Yellow, orange and red represents relatively high stain-absorbing structures such as nucleoli, green characterizes the nucleoplasm and grey defines the nuclear wall. Finally, the 3D reconstruction may be cropped to further examine internal structures that may be of interest. Fig. 2 illustrates tomographic reconstruction for an adenocarcinoma

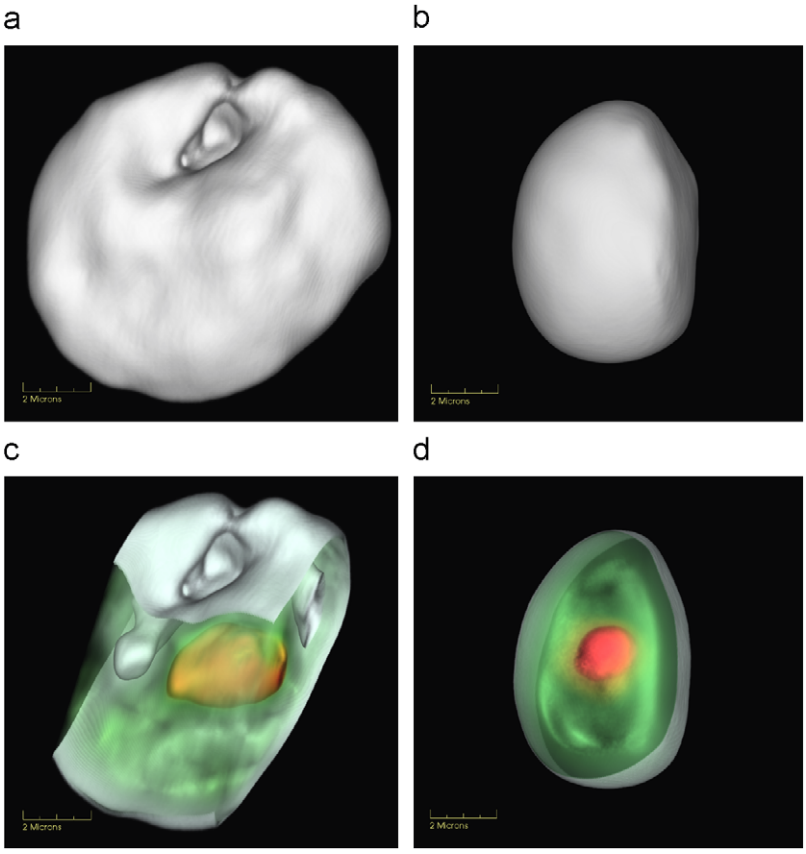

Fig. 2. Surface and cropped tomographic reconstructions for adenocarcinoma and normal epithelial cell nuclei. (a) Surface of an adenocarcinoma nucleus. (b) Surface of a normal epithelial nucleus. (c) Cropped translucent rendering of the adenocarcinoma nucleus of panel (a). (d) Cropped translucent rendering of the normal epithelial nucleus of panel (b). In panels (c) and (d), gray to green to orange to red represents increasing optical absorption.

cell nucleus and a normal cell nucleus. The reconstructions may also be examined through 360° of rotation in movies, Mov1, Mov2, Mov3 and Mov4 (see Appendix A).

4. Results

Results for the study are summarized in Figs. 3 and 4. Classifier sensitivity for 2D and 3D data sets were optimized for specificities of 90%, 93% and 96%. Cross-validated sensitivity was examined across all conditions to verify that the classifiers were not over-trained. Observations were made of the differences between the sensitivity using the whole training set and the sensitivity based on cross-validation results versus the number of features used in the classifier. Over-training is indicated when this difference systematically increases with a larger number of features. No systematic increase was noted for 2D or 3D classifiers. We therefore conclude that classifiers were not over-trained.

The bootstrap technique was used to estimate the average sensitivities for the 2D and 3D classifiers using between one and seven features. Bootstrapping was applied by sampling our data with replacement while maintaining the sample size for normal and adenocarcinoma at 148 and 178, respectively. A total of 1200 data sets were initially created. Thresholds for a desired specificity were computed for each data set. We desire the confidence interval for sensitivity given a constant specificity. Therefore, only those data sets of a consistent specificity near our target were accepted. The remaining data were down-sampled to ensure that 1000 data sets remained for all conditions studied.

Fig. 3 shows average sensitivity versus number of features for 96% specificity for 2D (red) and 3D (blue) classifiers. The figure shows

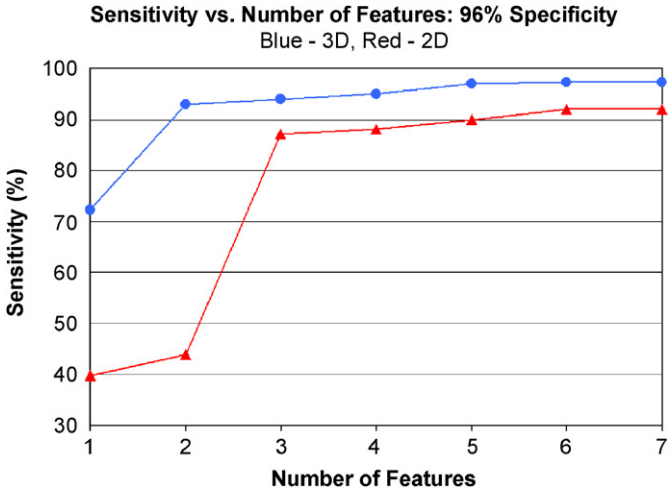

Fig. 3. Sensitivity versus number of features: 96% specificity. Shown are average sensitivities for 3D (blue) and 2D (red).

that sensitivity for 3D exceeds 2D for all feature levels. Wide differentials in sensitivity exist between 3D and 2D classifiers for one feature (the strongest feature) alone. The trend of Fig. 3 shows that asymptotic sensitivity was achieved for 2D and 3D classifiers using six features (of the 65 that were tested). More features are required to reach asymptotic sensitivity for 2D than for 3D, so that two-feature sensitivity for 3D exceeds six-feature sensitivity for 2D.

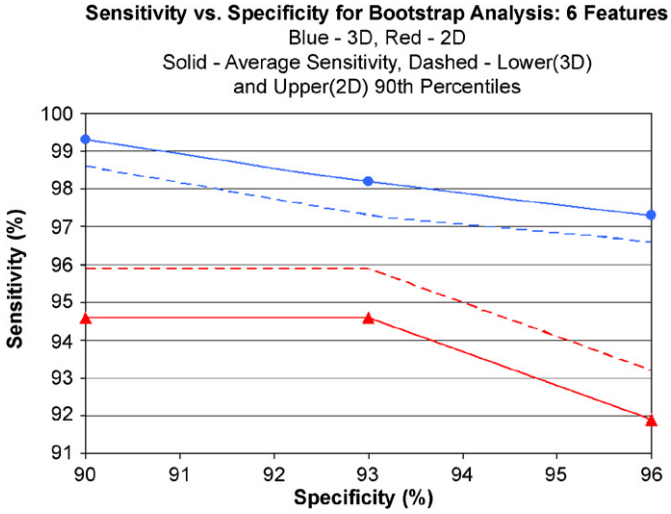

Fig. 4. Sensitivity versus specificity for bootstrap analysis: six features. Shown are 3D (blue)—average and lower 90th percentile sensitivity; 2D (red)—average and upper 90th percentile sensitivity.

Table 2
Most important features for 2D and 3D classifiers

2D features	3D features
Nuclear perimeter	Nuclear surface area
Small-sized texture for edge enhanced areas	Large-sized texture for edge enhanced volumes
Medium-sized texture for edge enhanced areas	

The bootstrap technique was further used to estimate the following data points at 90%, 93% and 96% specificity. For the 2D classifier, the upper 90th percentile for sensitivity was determined. The upper and lower 90th percentiles defined the range that included 90% of all performance estimates. Thus 5% of the performance estimates were above the upper 90th percentile and 5% were below the lower 90th percentile. Therefore, there was only a 5% chance that the performance was above the upper 90th percentile. For the 3D classifier, the lower 90th percentile for sensitivity was determined. Consequently, there was only a 5% chance that the performance was lower than the 90th percentile.

These data are plotted in Fig. 4. The 3D and 2D classifiers are again represented in blue and red, respectively. Solid lines represent the average sensitivity, and dashed lines represent the 90th percentile limits for sensitivity.

Fig. 4 shows a substantial differential in average sensitivity between the 2D and 3D classifiers that increases with specificity. Moreover, the figure shows no overlap between the lower 90th percentile for 3D and the upper 90th percentile for 2D. Therefore, performance of cell classification for 3D is improved over 2D with statistical significance. Average sensitivities at 96% specificity for 3D and 2D are 97.3% and 91.9%, respectively. Looking instead at the residual false negatives, the 3D performance improvement corresponds to $8.1/2.7 = 3$, or conversely, 2D produces a threefold increase in false negatives. Moreover, in an automated, rare-event cancer-detection paradigm, where high specificity is essential, the critical improvement in sensitivity achieved with 3D analysis may be acceptable, whereas 2D is not.

Table 2 shows a comparison of the first three features used for the classifier for 2D and the first two features for the classifier for 3D, both at 96% specificity, and demonstrates consistency in feature selection between the classifiers for 2D images and 3D tomographic reconstructions.

5. Summary

This study provides a validation for an automated lung cancer screening concept involving analysis of 3D tomographic reconstructions of cells. The study has demonstrated the superior merit of automated classification using 3D nuclear features relative to their 2D counterparts. However, this study is of limited scope, and is not necessarily representative of all the factors that would shape performance in a commercial screening instrument. Looking forward, we identify various factors that will receive further study and optimization.

- The study was performed using nuclei from lung adenocarcinoma and normal lung epithelial cell lines. While these cell lines derive from single human donors, this should not be seen as a limitation to the generalization of the results since normal and cancer cell morphology is independent of the host [13,14]. The next, clinical phase of research will determine how 3D classification performs on whole cells from sputum samples that have been collected from a broad patient population that encompasses the spectrum of lung normal, dysplastic and cancerous conditions.
- Cell preparation may not have been optimal for this study; however, it was consistent for all cells studied.
- Various parameters associated with the Cell-CT, such as condenser and objective NA, camera dynamic range, etc., may still require optimization.
- Features used in the 2D classifier respond to finer texture than their 3D counterparts. The 3D resolution for the Cell-CT system has been established at 0.9 μm and, given the system objective and condenser NA values, it is likely that 2D resolution is somewhat better than that. Therefore, it is likely that nuclei are rendered with higher resolution in 2D than in 3D. Consequently, Figs. 3 and 4 suggest that the more comprehensive morphological representation of nuclei in 3D trumps resolution as a determining factor for classification performance and that performance in 3D may be further enhanced by improving system resolution.
- By representing nuclei in 3D we eliminate classification errors arising from the perspective and focal plane position issues inherent in 2D imaging under a microscope. One may think, for example, of the characterization of nucleoli. Nucleoli may overlap in 2D, making an accurate count of these structures problematic. Preliminary studies, still in progress, demonstrate this effect and show greater likelihood for errors in 2D classification for structures that are complex. Therefore, errors in 2D-based classification are more likely to be made, for example, for an adenocarcinoma nucleus than for its relatively featureless normal counterpart.
- This study has largely explored features that have known significance from 2D cytology. The 3D imaging opens a larger, more comprehensive multidimensional feature domain for development. In fact, some potentially useful features only have a 3D definition. Returning to the consideration of nucleoli: in 2D it is not possible to determine where, relative to the nuclear wall, a nucleolus is located, whereas 3D Cell-CT solves this problem and allows distinction of a nucleolus from other condensed chromatin structures, such as a Barr body [15]. Moreover, a cell biology literature is emerging that proposes features that may only be observable in 3D, such as nuclear invaginations [16]. These features may be beneficial for the cancer-detection problem.

This report provides a strong motivation to pursue classification in 3D as a technical method with broad research applications in the biological sciences, including drug discovery and rare-event screening. Such rare-event screening may provide a key to a low cost method for routine screening for pre-invasive disease in the lung, the detection of which would foster early treatment with a greater

likelihood for curative success and perhaps open the door to preventive therapies.

Acknowledgement

We wish to think Dr. David Gur, University of Pittsburg Medical Center, for statistical advice and help with the manuscript.

Appendix A. Supplementary data

Supplementary data associated with this article can be found in the online version at 10.1016/j.patcog.2008.06.018.

References

[1] A. Kak, M. Slaney, Principles of Computerized Tomographic Imaging, IEEE Press, Piscataway, NJ, 1988 pp. 49–112.
[2] M. Fauver, et al., Three-dimensional imaging of single isolated cell nuclei using optical projection tomography, Opt. Express 13 (2005) 4210–4223.
[3] W. Smith, Modern Optical Engineering, third ed., McGraw-Hill, New York, 2000 pp. 156–157.
[4] B. Alberts, A. Johnson, J. Lewis, M. Raff, K. Roberts, P. Walter, The Cell, fourth ed., Garland Science, New York, 2002 pp. 561–565.
[5] J. Pawley, Handbook of Biological Confocal Microscopy, second ed., Plenum Press, New York, 1995 pp. 1–14.
[6] J. Frost, The Cell in Health and Disease. Monographs in Clinical Cytology, second ed., Karger, Basel, 1986.
[7] R. Jain, R. Kasturi, B. Shunck, Machine Vision, McGraw Hill, New York, 1995 pp. 40–47.
[8] P. Allison, Logistic Regression Using the SAS System, SAS Institute, Cary, NC, 1999 pp. 5–21.
[9] H. White, A. Gallant, K. Hornik, M. Stinchcombe, J. Wooldridge, Artificial Neural Networks, Blackwell Publishers, Cambridge, 1992 pp. 167–168.
[10] R. Haralick, L. Shapiro, Computer and Robot Vision VII, Addison-Wesley, Reading, MA, 1993 p. 605.
[11] C. Chen, P. Wang, Pattern Recognition and Computer Vision, third ed., World Scientific, New Jersey, 2005 p. 315.
[12] B. Efron, R. Tibshirani, Bootstrap methods for standard errors, confidence intervals, and other measures of statistical accuracy, Stat. Sci. 1 (1986) 54–75.
[13] G. Papinicolaou, H. Traut, Diagnosis of Uterine Cancer by the Vaginal Smear, Harvard University Press, Cambridge, 1943.
[14] L. Koss, M. Melamed, Koss' Diagnostic Cytology and its Histopathologic Bases, fifth ed., Lippincott Williams and Wilkins, Philadelphia, 2006.
[15] M. Barr, E. Bertram, A morphological distinction between neurons of the male and the female, and the behaviour of the nucleolar satellite during accelerated nucleoprotein synthesis, Nature 163 (1949) 676.
[16] N. Johnson, et al., Actin-filled nuclear invaginations indicate degree of cell de-differentiation, Differentiation 71 (2003) 414–424.

About the Author—MICHAEL MEYER is currently Vice President for Image Engineering at VisionGate where he is supervising development of automated classification systems for detection of abnormal cells in sputum specimens. He is listed on six US patents and holds an MSEE from the University of Washington in Seattle.

About the Author—MARK FAUVER received his B.S. in Physics in 1993 from University of California, Los Angeles, and his M.S. in Bioengineering in 1996 from University of Washington in Seattle. His research interests include 3D microscopy, micromechanics, biomedical device design and micro-fabrication techniques. He served as research engineer and research scientist in various labs at University of Washington from 1997–2006. Mark served as Principle Engineering Scientist at VisionGate from 2006 to early 2008. He now works as a consultant for Nortis.

About the Author—J. RICHARD RAHN received his Ph.D. in Physics in 1996 from the University of Massachusetts (Amherst). He has been VisionGate's director for optical systems research since 2002. He holds two US patents, with several more applied for, and has published articles in optical spectroscopy and 3D imaging.

About the Author—THOMAS NEUMANN received his M.D. degree from the Martin-Luther University, Germany, in 1994. Afterwards, he took a position as Research Assistant Professor at the University of Washington in 2002. He joined VisionGate, Inc., as Vice President for Medical Sciences in 2004. His research interests include cell separation, automation of specimen preparation and biomedical device design.

About the Author—FLORENCE W. PATTEN received her B.S. (General Science) degree from the University of Oregon, Eugene, Oregon, MT(ASCP) in Medical Technology from the University of Oregon Medical School, Portland, Oregon, and CT(ASCP) in Cytotechnology from the University of Oregon Medical School, Portland, Oregon. She currently serves as the Vice President for Clinical Affairs, VisionGate, Inc., Gig Harbor, Washington.

About the Author—ERIC SEIBEL is a Research Associate Professor, Mechanical Engineering and Adjunct Bioengineering at the University of Washington. Dr. Seibel develops instrumentation based on optical scanning techniques that lead to early detection of disease. Before receiving his Ph.D., he worked four years in the medical device industry.

About the Author—ALAN NELSON has started two biomedical companies: NeoPath and VisionGate, serving as CEO. Dr. Nelson was a tenured Associate Professor of Bioengineering at the University of Washington, and before that he held the WM Keck Foundation endowed chair professorship at MIT. He holds 21 issued US patents and has published over 100 papers in the field of biomedical imaging.